Environmental Science & Technology

pubs.acs.org/est

Article

Molecular Dynamics Simulation Prediction of the Partitioning Constants (K_H, K_{iw}, K_{ia}) of 82 Legacy and Emerging Organic Contaminants at the Water−Air Interface

Amélie C. Lemay,*[,∥] Ethan J. Sontarp,[∥] Daniela Martinez, Philip Maruri, Raneem Mohammed, Ryan Neapole, Morgan Wiese, Jennifer A. R. Willemsen, and Ian C. Bourg

Cite This: *Environ. Sci. Technol.* 2023, 57, 6296−6308

Read Online

ACCESS | Metrics & More | Article Recommendations | Supporting Information

ABSTRACT: The tendency of organic contaminants (OCs) to partition between different phases is a key set of properties that underlie their human and ecological health impacts and the success of remediation efforts. A significant challenge associated with these efforts is the need for accurate partitioning data for an ever-expanding list of OCs and breakdown products. All-atom molecular dynamics (MD) simulations have the potential to help generate these data, but existing studies have applied these techniques only to a limited variety of OCs. Here, we use established MD simulation approaches to examine the partitioning of 82 OCs, including many compounds of critical concern, at the water−air interface. Our predictions of the Henry's law constant (K_H) and interfacial adsorption coefficients (K_{iw}, K_{ia}) correlate strongly with experimental results, indicating that MD simulations can be used to predict K_H, K_{iw}, and K_{ia} values with mean absolute deviations of 1.1, 0.3, and 0.3 logarithmic units after correcting for systematic bias, respectively. A library of MD simulation input files for the examined OCs is provided to facilitate future investigations of the partitioning of these compounds in the presence of other phases.

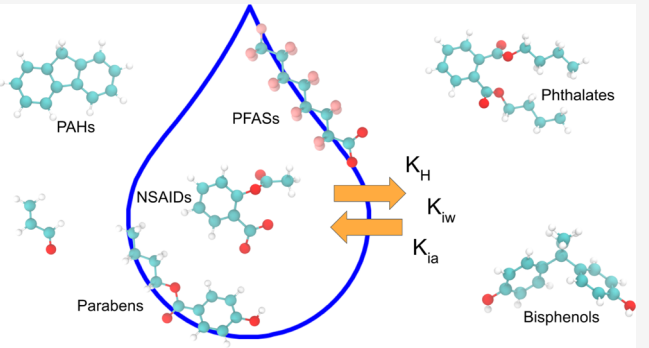

KEYWORDS: *adsorption, PFAS, phthalate, PCB, PAH, paraben, micropollutant, aerosol*

INTRODUCTION

A key hindrance to the mitigation of organic contaminants (OCs) is insufficient knowledge of the thermodynamic constants that reflect their affinity for different phases and interfaces in natural and engineered systems.[1−9] This limited availability of fundamental thermodynamic data reflects a widening gap between, on the one hand, the ability of regulatory agencies to carry out experimental characterizations of substances that can be highly hazardous or challenging to synthesize and, on the other hand, the rapidly increasing diversity of OCs illustrated by the nearly 70 000 chemicals or mixtures registered globally in the past decade[10,11] or by the nearly 4000 applications for regulatory approval submitted to the US Environmental Protection Agency (EPA) between 2016 and 2021.[12]

Efforts to predict the partitioning of OCs in natural and engineered systems have focused primarily on the development of approaches that rely on correlations against various properties of individual OC molecules (including chemical formula, functional groups, size, conformation, polarity, and other properties predicted using various levels of refinement up to quantum chemical calculations) trained using pre-existing partitioning data.[3,13−18] Alternatively, the well-established COSMOtherm approach relies on quantum mechanical simulations of individual organic solutes carried out using a dielectric continuum approximation for the solvent.[19,20] Efforts to cross-validate and benchmark existing approaches such as SPARC, COSMO*therm*, SIMPOL.1, and poly-parameter linear free energy relationships (ppLFERs) indicate that, for water−air partitioning and related properties (e.g., saturation vapor pressure), these approaches differ from each other and from experimental results by ∼1 order of magnitude for sparsely functionalized, weakly soluble compounds.[3,21,22] For more soluble, highly functionalized compounds (properties common to many contaminants of emerging concern),[23] however, different well-established approaches deviate by up to 10 orders of magnitude, and their predictive utility is therefore highly uncertain.[3]

Received: January 10, 2023
Revised: March 22, 2023
Accepted: March 23, 2023
Published: April 4, 2023

https://doi.org/10.1021/acs.est.3c00267
Environ. Sci. Technol. 2023, 57, 6296−6308

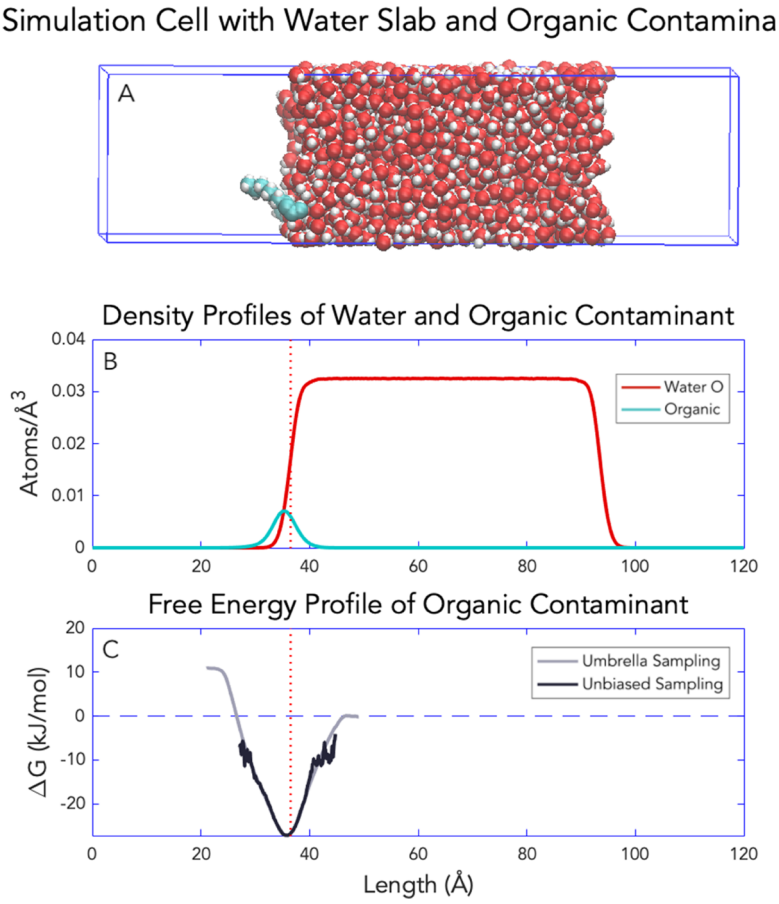

Figure 1. Illustration of our MD simulation methodology: (A) snapshot of a simulated system showing an organic molecule at the water−air interface (C, O, and H atoms in cyan, red, and white, respectively); (B) density profiles of water O atoms and organic atoms (blue and red lines) as a function of distance normal to the water−air interface (y) in a standard ("unbiased") MD simulation, averaged over 40 ns of simulation; (C) free energy profiles of the organic contaminant as a function of y determined either from the density profile of the organic molecule center of mass in an unbiased simulation (black line) or using the umbrella sampling (US) methodology (gray line).

All-atom molecular dynamics (MD) and density functional theory (DFT) simulations provide a potential alternative approach to filling the knowledge gap outlined above by enabling predictions of the partitioning behavior of environmental contaminants in explicitly simulated phases and multiphase systems. The promise of this approach is illustrated by its use in drug discovery and toxicology.[24−28] In the environmental sciences, increasing numbers of studies over the last two decades have used all-atom simulations to gain insight into the local coordination, energetics, and dynamics of OCs in natural systems.[29−35] However, few of these studies have generated information on the equilibrium constants controlling partitioning between phases or adsorption at interfaces.[36−42]

Here, we evaluate the feasibility of using all-atom MD simulations to generate thermodynamic data for OC partitioning in natural systems. We focus on systems containing water, air, and a water−air interface as a simple environmental multiphase system with important implications in contaminant fate and transport.[43−45] To evaluate OC partitioning, we create and test an open library of input files for a diverse set of 82 OCs. The compounds examined span those produced and released with minimal regulation prior to 1970 and categorized as legacy contaminants (benzene, formaldehyde, polychlorinated biphenyls, tetrachloroethylene, polycyclic aromatic hydrocarbons, etc.) to more recently produced and less regulated contaminants of emerging concern (nonionic surfactants, per- and polyfluoroalkyl substances, phthalates, pyrethroid pesticides, etc.) as well as ubiquitous pharmaceutical products (acetylsalicylic acid, ibuprofen, naproxen) and compounds naturally present at the water−air interface (acetic acid, glyoxal, isoprene). For each compound, we determine its Henry's law constant, K_H, and its interfacial adsorption coefficients from water and air, K_{iw} and K_{ia}. We compare our results with published experimental data to quantify the accuracy and precision of our predicted thermodynamic constants. Finally, we examine our simulation results to gain insight into the relation between these constants and the molecular structure of the organic compounds.

SIMULATION METHODOLOGY

Database of Organic Contaminants. The list of 82 compounds examined here is presented in Table SI1. This list contains similar numbers of legacy contaminants, for which experimental data exist to verify partitioning and adsorption at the water−air interface for many compounds, and contaminants of emerging concern, which the US EPA and National Science Foundation (NSF) have identified as key research priorities, for which fewer experimental data exist. The contaminants span those classified as per- and polyfluoroalkyl substances (PFAS), bioaccumulative endocrine disruptors detected in the blood of 98% of Americans;[46,47] nonsteroidal anti-inflammatory drugs (NSAIDs), ubiquitous pharmaceutical

https://doi.org/10.1021/acs.est.3c00267
Environ. Sci. Technol. 2023, 57, 6296−6308

chemicals detected in drinking and groundwater that can cause adverse ecotoxicological effects;[48,49] phthalates, plasticizers widely used in personal care products with known epigenetic and endocrine-disrupting toxicological effects;[50−52] polycyclic aromatic hydrocarbons (PAHs), a key category of carcinogenic and/or mutagenic compounds associated with combustion processes;[53−55] polychlorinated biphenyls (PCBs), a class of industrial persistent organic pollutants (POPs) that remains one of the predominant threats to water and air quality worldwide;[53−58] and multiple other compounds of concern in environmental or human health.[23,59−63] The list also includes seven compounds that are naturally present at or near the water−air interface, including biogenic semivolatile organic compounds that play important roles in aerosol chemistry and indoor air quality.[64,65]

Input files for the compounds in Table SI1 were developed using the OPLS-AA model, a general-purpose interatomic potential model widely used for MD simulations of systems containing organic compounds and liquid water.[66,67] The OPLS-AA model represents the potential energy of organic-water systems as a sum of pairwise van der Waals and Coulomb interactions (represented, respectively, using the Lennard-Jones 6−12 model and a fixed partial charge for each atom) as well as contributions associated with intramolecular bond lengths, angles, and torsions. For compounds that carry ionizable groups, the protonation state was selected to represent the predominant species at pH 7. For compounds that contain uncommon atom linkages for which bond, angle, or torsion parameters do not exist in the OPLS-AA model, the parameters for the most similar linkages were used as noted in the comments of the input file for each compound. The program Moltemplate[68] was used to develop the compound input files. A database of input files for carrying out MD simulations of the compounds in Table SI1 using the open-source program LAMMPS[69] is available at [https://github.com/amelielemay/MD-Contaminants].

Molecular Dynamics Simulations. Simulations were carried out using the code LAMMPS on the Cori supercomputer at the National Energy Research Scientific Computing Center (NERSC) and on the Tiger CPU cluster at Princeton University. The simulation cell size was 32 × 120 × 32 Å^3 with periodic boundary conditions in all directions. Simulated systems contained a 60-Å-thick slab of liquid water (5700 water molecules) adjacent to a 60-Å-thick slab of void space, with a single organic molecule located near one of the water−air interfaces (Figure 1A). For charged compounds, charge balance was ensured by the addition of Na^+ or Cl^- counterions. To prevent the location of the water−air interface from drifting during the simulations, the overall center of mass of the water O atoms was fixed in the y direction. In addition, a 10-Å-thick reflective wall was placed in the void space at each end of the simulation cell to prevent evaporated water molecules from drifting to the neighboring periodic image of the simulation cell in the y direction. Simulations were carried out in the canonical (NVT) ensemble at a temperature of 298 K using a Verlet algorithm with a timestep of 1 fs. Interatomic interactions were resolved in real space up to a cutoff of 15 Å. Coulomb interactions beyond this cutoff were resolved in reciprocal space using the particle−particle, particle mesh (PPPM) method[70] with a precision of 99.9%. Water molecules were kept rigid using the SHAKE algorithm.[71]

Molecular dynamics simulations solve Newton's equations of motion for a many-particle system using semiempirical interatomic potential parameters.[72] As such, simulation predictions are sensitive to the choice of interatomic potential model. Here, we used the OPLS-AA model for organic molecules,[66] the Dang−Smith model for Na^+ and Cl^-,[73] and the simple point charge (SPC) model for water.[74] These models have been extensively used to predict the conformation and coordination of organic compounds in water.[28,75,76] The few existing comparative studies on the relative ability of different interatomic potential models to predict organic compound partitioning at the water−air interface suggest that the combination of the SPC and OPLS-AA models is among the most accurate.[36,76−78] To gain insight into the sensitivity of the simulation predictions to the choice of interatomic potential models, a subset of the simulations was repeated using the extended simple point charge (SPC/E) water model (Figure SI4).[79] Future investigations should more extensively characterize the sensitivity of simulation predictions to the choice of interatomic potential models, including other general-purpose organic models such as AMBER,[80] CHARMM,[81] and GROMOS[82] and other water models such as TIP4P2005.[83]

Calculation of the Free Energy Profile. Two methods were used to determine the free energy (FE) profile of OCs as a function of distance from the interface. In the first method, applied for a subset of the simulated compounds, standard ("unbiased") MD simulations were carried out with the OC initially located near one of the interfaces. Simulations were equilibrated for 423 ps in the NVT ensemble, after which production runs were carried out for 40 ns in the same ensemble. Average density profiles of water O atoms (ρ_{OW}) and of the center of mass of the organic molecule (ρ_{OM}) were determined as a function of y (Figure 1B). Finally, the FE of the organic compound as a function of y, relative to an arbitrary reference, was calculated as $\Delta F \propto -RT \ln \rho_{OM}$. The resulting ΔF values, obtained in the NVT ensemble, are Helmholtz free energies, but they are essentially identical to Gibbs free energies as $P_y \approx 0$ in our simulated systems. As illustrated by the black line in Figure 1C, a limitation of the resulting FE profiles is their limited extent in the y direction, as the unbiased method only yields precise estimates of FE in the narrow range of y values that is extensively sampled by the organic molecule.

To characterize the FE profiles of organic compounds in a wider range of y coordinates spanning the two bulk fluids, we used the umbrella sampling (US) method, a "biased" MD simulation approach.[37,38,77,84] In the US method, a harmonic biasing potential is used to tether the compound to a certain reaction coordinate. The resulting analysis yields the FE profile in the vicinity of the tethering location. The method is repeated for different tethering locations. Finally, the results of the different biased simulations are combined using an iterative calculation, the weighted histogram analysis method (WHAM), that determines the optimal offsets between the FE profile sections obtained with different tethering locations.[85] In this study, each compound was tethered to a range of y coordinates that spanned from bulk air to bulk water. The tethering locations were separated by intervals of 2 Å. Each simulation was preceded by 9.2 ps of equilibration with no biasing potential, 13 ps of equilibrium during which the harmonic force constant was increased to 0.1 eV Å^{-2}, and 400 ps of equilibration with a fixed harmonic force constant of 0.1 eV Å^{-2}. Finally, production runs were carried out for 40 ns with a minimum of 11 tethering locations, such that each FE

https://doi.org/10.1021/acs.est.3c00267
Environ. Sci. Technol. 2023, 57, 6296−6308

profile required at least 440 ns of simulation. Results obtained with different tethering locations were combined using 10^4 iterations of the WHAM algorithm. A representative example of the resulting free energy profiles is shown as a gray line in Figure 1C.

RESULTS AND DISCUSSION

Free Energy Profiles. Predicted FE profiles for the 82 compounds examined here are presented in Figure SI1. Profiles are reported as average values calculated over 40 ns of simulation at each tethering location, with error bands indicating the precision (95% confidence intervals) evaluated by dividing each 40 ns simulation into four 10 ns intervals. Reported FE profiles were normalized relative to the average value in bulk water, defined as the FE plateau in the 1 Å range of y coordinates immediately below the maximum tethering location. Profiles are also reported for a subset of the compounds in Figure SI2 based on unbiased simulations. For all compounds for which both US and unbiased simulations were carried out, good agreement was observed between the shapes of the FE minima determined by both methods.

Several notable trends emerge from the collection of ΔF profiles in Figure SI1. First, almost all compounds examined here exhibit surfactant-like properties with a FE minimum in the vicinity of the water−air interface. This minimum had an average depth of 15.0 ± 7.6 kJ mol^{-1} relative to the value in bulk water (where the range reflects $\pm\sigma$, where σ is the standard deviation (SD) of the 75 values with FE minima at the interface) and was located 0.3 ± 0.8 Å above the water surface. This minimum indicates that most compounds examined here exhibit a strong preference (relative to both bulk water and air) for being located at the interface, where they can form favorable interactions with water molecules without strongly disrupting the water hydrogen bond network.

Second, the FE profiles of charged compounds do not stabilize in the vapor phase, as shown in Figure 2, indicating that exsolution of ionic species is highly unfavorable. The three zwitterions in the database (glyphosate, glufosinate, PFAS-5-3-FtB) also did not reach a stable ΔF value in the air phase. Although we are not aware of any previous reports of the free energy profiles of organic ions or zwitterions across the water−air interface, such a profile was reported recently for Cl^- at a flat water−air interface[86] and previously for Cl^- at water−organic liquid interfaces[87,88] These results indicated that the free energy profile of Cl^- only begins to stabilize at distances >15 Å beyond the water surface and that accurate sampling of the free energy is complicated by hysteresis in the formation of water fingers and the residual hydration of the ion in air. For this reason, the Henry's law constant (K_H) and the adsorption constant relative to air (K_{ia}) were not determined for the charged compounds, and only the adsorption constant relative to water (K_{iw}) is reported for these compounds. This finding is consistent with the expectation that, for compounds that exist predominantly in ionized form in liquid water, measured K_H values reflect the exsolution of the less predominant uncharged form.[6] Prediction of such K_H values using the methodology used here (where molecules cannot spontaneously gain or lose protons) would require simulating the uncharged form of these compounds and adjusting the predicted FE of evaporation to account for their FE of protonation or deprotonation. For compounds that have pK_a values near 7, our predicted K_{iw} and K_{ia} values should be treated with caution as the protonation state of organic compounds may vary in the vicinity of the water−air interface.[89,90]

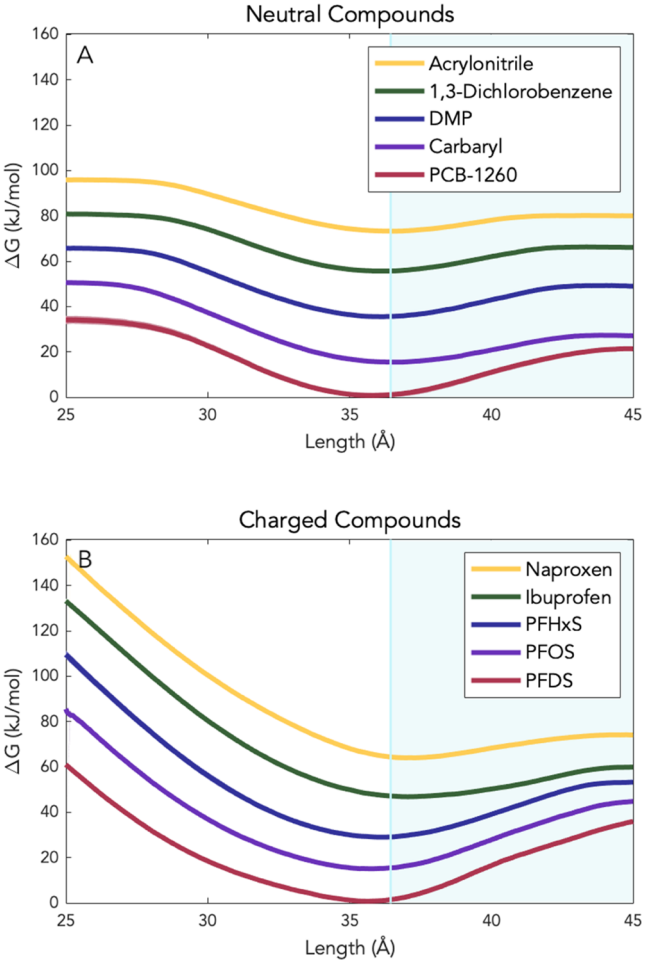

Figure 2. Representative subset of FE profiles obtained for neutral and charged compounds (upper and lower panels, respectively). The uncharged compounds display an FE plateau in both phases at distances about 10 Å above or below the water surface (located at y = 36.45 Å). For the charged compounds, a plateau is not observed in the vapor phase on the length scales examined by our simulations.

Third, 32% (26 of 82) of the profiles exhibit a ΔF barrier of at least 0.25 kJ mol^{-1} located about 5 Å below the water surface, as reported in some previous MD simulation studies.[37,91] This barrier indicates the existence of an organic-depleted region on the water side of the interface, near the location of the second monolayer of water molecules at the interface,[92] with possible implications for mass transfer and chemical transformation kinetics of organic compounds at the water−air interface.[93] A full list of the compounds exhibiting such a barrier is given in Table SI2, and a subset is shown in Figure 3.

Partitioning between Water and Air. The Henry's law solubility constant, K_H, is the quotient of the concentration of a dissolved compound in water (mol m^{-3}) and its partial pressure in air (Pa) in the limit of infinite dilution. We determined the value of this constant for each of the compounds in our library from its FE of evaporation, $\Delta F_{evap} = \Delta F_a - \Delta F_w$. The FE in bulk air, ΔF_a, was calculated as the average value in the 1-Å-wide range of y values directly above the minimum tethering location, while the FE in bulk water, ΔF_w, was calculated as the average value in the 1-Å-wide range

https://doi.org/10.1021/acs.est.3c00267
Environ. Sci. Technol. 2023, 57, 6296−6308

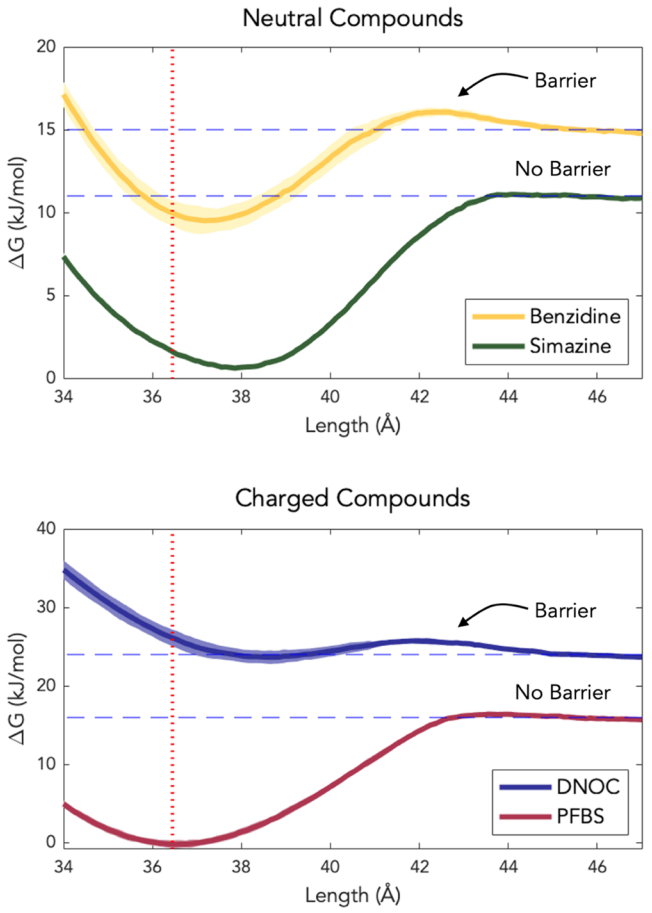

Figure 3. Representative subset of FE profiles exhibiting an energy barrier between the FE minimum at the interface (near the Gibbs dividing surface of water at y = 36.45 Å, indicated as a vertical dashed line) and the FE plateau in bulk liquid water (around 45 Å).

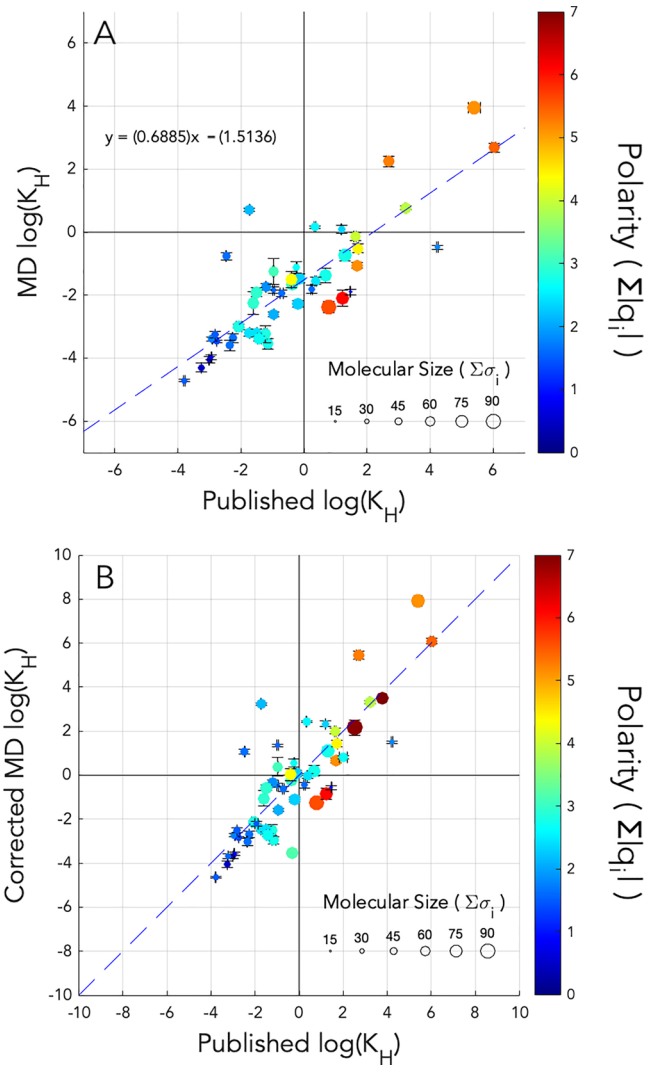

Figure 4. Predicted vs average measured log(K_H) values (with K_H in mol m^{-3} Pa^{-1}) based on (A) MD simulation results and (B) bias-corrected MD simulation results. The error bars indicate 95% confidence intervals on the predicted and average measured values. As rough scales for the polarity and size of simulated OCs, we use the sum of the magnitudes of the partial charges and van der Waals radii, respectively, of the atoms in the OPLS-AA model of each organic molecule.

of y values directly below the maximum tethering location. The Henry's law solubility constant was then calculated as $K_H = (1/RT) \times \exp(\Delta F_{evap}/RT)$, where T is the absolute temperature (298 K) and R is the ideal gas constant. Our predictions of K_H are reported as log(K_H), with 95% confidence intervals calculated as $2\sigma/\sqrt{n}$, where σ is the SD of predicted log(K_H) values estimated from n = 4 distinct FE profiles calculated from the four 10 ns intervals of each simulation. Our predicted values of log(K_H) are compiled in Table SI1.

To evaluate the potential existence of a systematic bias in our MD simulation predictions of log(K_H), predicted values are presented in Figure 4A as a function of the extensive database of log(K_H) values compiled by Sander.[94] The values from the Sander compilation used here were those listed as being most reliable, designated in the compilation with an M, L, or V. Confidence intervals were assigned to the Sander values as $2\sigma/\sqrt{n}$, where n is the number of reliable K_H values listed for each compound and σ = 0.190 is the estimated SD of experimental log(K_H) values, computed as the average SD of log(K_H) for the 10 compounds with the most reported K_H values in Sander's database. Compounds with no highly reliable experimental K_H values in Sander's database are omitted from Figure 4. Compounds for which approximations in atoms linkages or charges were made because there were no existing parameters in the OPLS-AA database (as indicated in Table SI1) were omitted from Figure 4A and the calculation of the regression line (they are included in Figure 4B). Finally, decabromodiphenyl ethane (DBDE) was excluded from both plots because it is an outlier that differs from the experimental value by 6.36 log units. This molecule also differs from others in our dataset by its high abundance of aromatic C−Br linkages, suggesting that the OPLS-AA parameters for this functional group may require further evaluation.

Linear regression of the results presented in Figure 4A reveals a systematic bias between the values predicted by our simulations and the measured values characterized by the relation log($K_{H,predicted}$) = 0.6885 × log($K_{H,measured}$) − 1.5136. In short, MD simulations carried out using the SPC and OPLS-AA interatomic potential models tend to underestimate the affinity of organic compounds for water vs air, particularly for more hydrophilic compounds. Most of this bias likely reflects the approximate nature of the interatomic potential models. However, part of it could possibly be associated with the experiments; for example, measurements using the inert gas stripping method have been found to overestimate K_H, in some

https://doi.org/10.1021/acs.est.3c00267
Environ. Sci. Technol. 2023, 57, 6296−6308

cases by several orders of magnitude, if their interpretation does not account for adsorption at the water−air interface.[8,17,95,96]

Results presented in Figure 4A suggest that MD simulation predictions of $\log(K_H)$ obtained with the OPLS-AA and SPC models can be empirically corrected for their systematic bias using the relation $\log(K_{H,corrected}) = [\log(K_{H,predicted}) + 1.5136]/0.6885$. The resulting bias-corrected simulation results, presented in Figure 4B, match the average measured $\log(K_H)$ values with a mean absolute difference (MAD) of 1.1 logarithmic units. The accuracy and precision of our simulation predictions (reflected by the systematic bias and by the MAD after bias correction) are commensurate with those reported for established methods used to predict $\log(K_H)$. For example, a comparison of $\log(K_H)$ values predicted using SPARC, COSMO*therm*, and ppLFER approaches for natural organic compounds with 0 to 3 functional groups (consistent with most compounds examined here) yielded an average MAD of 1.5 log units between different approaches,[3] implying an MAD of at least 0.8 log units between the predictive models and experimental results.

The outliers for which our bias-corrected simulation predictions deviate from the experimental values by three or more logarithmic units are hexachlorobenzene (−1.73, 3.23), 1,3-dichlorobenzene (−2.47, 1.08), and clofenotane (DDT) (−0.325, −3.54). DDT is a compound for which charge adjustments and atom type substitutions were made as it contains unusual combinations of functional groups for which OPLS-AA model parameters are not available. Our results suggest a need to develop OPLS-AA parameters for this compound. The mismatch observed for hexachlorobenzene and 1,3-dichlorobenzene is unexpected as no adjustments were made for these compounds. The other benzene derivatives (benzene, ethylbenzene, 1,2- and 1,4-dichlorobenzene, toluene, 4-chlorophenyl, and 4-bromophenyl phenyl ether) match the experimental data well; therefore, we cannot conclusively state why two of the benzene-derived compounds deviate from the experimental values.

Adsorption at the Water−Air Interface. The interfacial adsorption coefficients, K_{iw} and K_{ia}, are the quotients of the surface excess of a compound at the water−air interface, Γ_i (mol m^{-2}), and its concentration in bulk water or air, C_w or C_a (mol m^{-3}), respectively. The interfacial surface excess Γ_i is conventionally defined relative to the Gibbs surface of water using the relation

$$\Gamma_i = \int_{y_{min}}^{y_{max}} \rho_{OM}(y)\, dy - (y_{max} - y_i)C_w - (y_i - y_{min})C_a \quad (1)$$

where $\rho_{OM}(y)$ is the density profile of the organic compound as a function of distance in the direction normal to the interface, y_i is the location of the Gibbs surface of water (i.e., the interface location imposed such the surface excess equals zero for water), and y_{min} and y_{max} are coordinates in bulk air and bulk water. Based on eq 1 and the Boltzmann relation $\rho_{OM} \propto \exp(-\Delta F/RT)$, the interfacial adsorption coefficient $K_{iw} = \Gamma_i/C_w$ is obtained from the FE profile through the relation

$$K_{iw} = \int_{y_{min}}^{y_{max}} e^{-((\Delta F(y) - \Delta F_w)/RT)}\, dy - (y_{max} - y_i) - (y_i - y_{min})e^{-(\Delta F_{evap}/RT)} \quad (2)$$

The interfacial adsorption coefficient $K_{ia} = \Gamma_i/C_a$ is determined in an analogous manner. The integrals in eqs 1 and 2 were evaluated from predicted FE profiles using a small-rectangle approximation with a bin width of 0.1 Å. Results are presented in Table SI1.

Experimental values of K_{iw} and K_{ia} are far less commonly reported in the literature than K_H. A literature search for experimental K_{iw} and K_{ia} values of the compounds in our database resulted in 11 and 10 values, respectively. We chose not to convert between published K_{iw} and K_{ia} values using the relationship $K_H RT = K_{iw}/K_{ia}$ due to the uncertainty associated with K_H values for compounds for which there are few experimental data. Additionally, we excluded 1,3-dichlorobenzene from our comparison and regression computation, as it is one of the three outliers in Figure 4B.

Published $\log(K_{iw})$ values for six compounds (benzene, ethylbenzene, toluene, 1,1,1-trichloroethane, tetrachloroethylene, trichloroethylene) as reported by Hoff[97] (based on a gas chromatography-based method that measures K_{iw} and K_{ia} simultaneously) and for four PFAS (PFOA, PFOS, PFBS, PFHxS) as compiled by Brusseau[98] (based on surface tension measurements) are compared with our simulation predictions in Figure 5A. Experimental $\log(K_{ia})$ values for nine compounds (benzene, ethylbenzene, 1,2-dichlorobenzene, 1,4-dichlorobenzene, toluene, tetrachloroethylene, 1,1,1-trichloroethane, 1,4-dioxane, trichloroethylene) reported by Hoff et al.[97] and Kelly et al.[99] are compared with our simulation predictions in Figure 5B.

Results shown in Figure 5A reveal that our predicted $\log(K_{iw})$ values are consistent with experimental results, with a MAD of 0.5 log units prior to bias correction. A regression line plotted through both PFAS and legacy compounds is statistically consistent with a 1:1 relationship (slope of 1.3 ± 0.6, intercept of 1.3 ± 2.6, reflecting the $t_{0.975,\, n-2}$ confidence intervals). If PFAS and legacy compounds are considered separately, our MD simulation results tend to overestimate reported $\log(K_{iw})$ values for the former and underestimate $\log(K_{iw})$ for the latter. This may reflect a bias in our simulations associated with the OPLS-AA model parameterizations of C−F, C−H, and C−Cl bonds. Alternatively, it also may reflect a bias in the experimental database due to the different methodologies used to measure $\log(K_{iw})$ values for PFAS vs legacy contaminants in Figure 5A.

Results shown in Figure 5B indicate that predicted $\log(K_{ia})$ values generally underestimate the experimental values, with a mean difference of −1.4 logarithmic units. Linear regression of the results in Figure 5B yields a slope of 0.5 ± 0.2 (intercept of −3.4 ± 0.8), which indicates that the simulations increasingly underestimate $\log(K_{ia})$ with increasing compound hydrophilicity. In short, our simulations underestimate the propensity of OCs to adsorb from the air phase onto the surface of liquid water, particularly for the more hydrophilic compounds.

Overall, our results shown in Figure 5 suggest that the systematic bias in predicted $\log(K_H)$ values in Figure 4A results from an underestimation of the tendency of OCs (and particularly of hydrophilic OCs) to adsorb from air onto the water surface, whereas the simulations correctly predict the partitioning of OCs between the interface and bulk water. This finding is consistent with the fact that the OPLS-AA model was developed to represent organic compounds in condensed phases (such as water, hydrocarbon fluids, biological matrices) rather than in gas phases.[100]

https://doi.org/10.1021/acs.est.3c00267
Environ. Sci. Technol. 2023, 57, 6296−6308

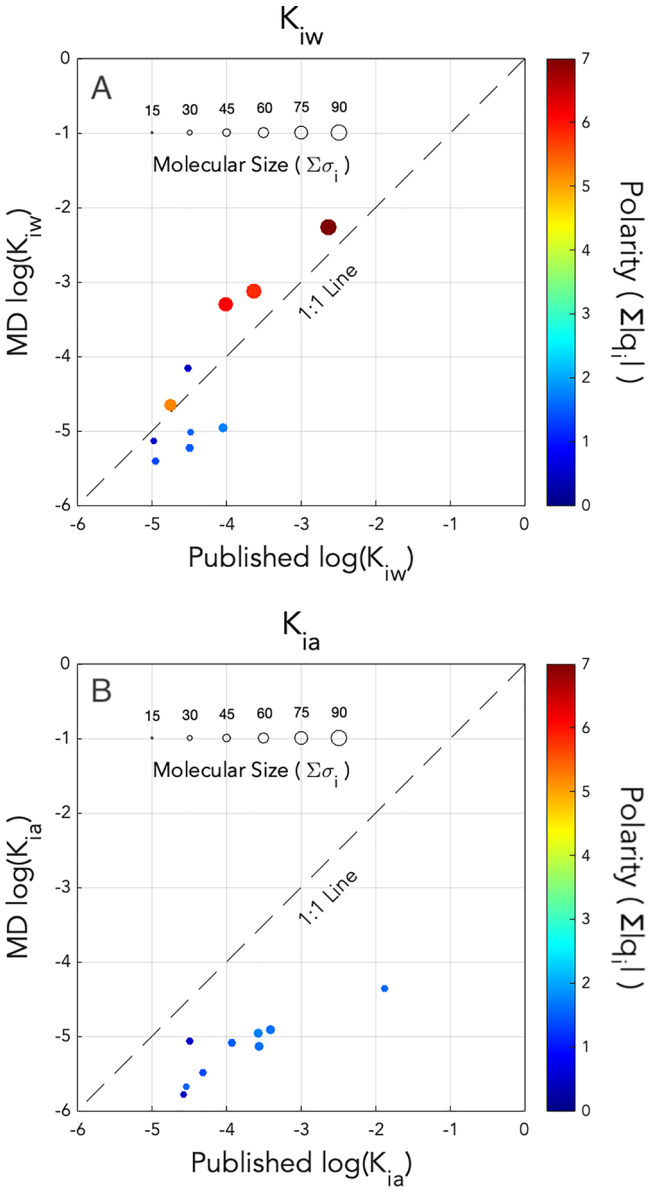

Figure 5. Predicted vs measured log(K_i) values (with K_i in cm) based on (A) interfacial-water coefficients (K_{iw}) and (B) interfacial-air coefficients (K_{ia}).

We note, in passing, that our log(K_{iw}) results for PFAS shown in Figure 5A may help resolve a debate regarding the suitability of the Langmuir and Freundlich isotherms for PFAS adsorption at the water−air interface.[98,101−104] The consistency of our predictions with the low-salinity, low-concentration results compiled by Brusseau[98] suggests the existence of a finite log(K_{iw}) value at infinitely low loading, in agreement with the Langmuir model.

Sensitivity to the Interatomic Potential Models. As a preliminary evaluation of the sensitivity of our predictions to the choice of interatomic potential model, seven of the compounds in our library were simulated using the SPC/E water model in addition to the SPC model. The only difference between the SPC and SPC/E water models is that the latter assigns 3% larger partial charges to water O and H atoms, resulting in a larger dipole moment and stronger hydrogen bonds. Free energy profiles predicted with the two water models are compared in Figure SI2. Our results show that the SPC model yields higher log(K_H) values and lower or similar log(K_{iw}) values, with mean differences of 0.4 and −0.5 logarithmic units, respectively. In other words, the SPC/E model predicts a smaller affinity of OCs for bulk water. Log(K_H) values predicted using the SPC model more closely match experimental values for five of the six compounds with reliable published values.

Implications for Environmental Partitioning. The environmental implications of our K_H and K_{iw} values are illustrated in Figure 6, a partitioning space plot indicating the phase or interface that holds the largest quantity of each compound in a generic warm cloud at 298 K. Dashed lines delineate regions in log(K_H)−log(K_{iw}) space where the associated compounds have greater total abundance in water, air, or at the interface, which depend on the relative values of water volume V_{water}, air volume V_{air}, and water−air interfacial area $A_{interface}$ in the system of interest. A representative warm cloud was assumed to have an aqueous phase consisting of spherical droplets with a radius of 10^{-5} m and a volume fraction of water of 3×10^{-7} m^3/m^3.[105] The charged compounds, for which exsolution is so unfavorable that K_H could not be quantified, are drawn as red symbols near the right edge of the diagram.

In a warm cloud, most neutral compounds are predicted to be located predominantly in air due to the large abundance of this phase. Seven neutral compounds are located predominantly in water (bisphenol-A, benzidine, 2,4,6-trinitrotoluene, *N*-methylpyrrolidone, methylparaben, simazine, carbaryl, hexachlorobenzene), although we note that the last compound shows an unexpectedly large log(K_H) value according to Figure 4B. Two neutral compounds are predicted to be located predominantly at the water−air interface (4-nonylphenol diethoxylate, cyfluthrin).

The charged compounds, conversely, are all predominantly located in bulk water or at the interface, with different adsorbed fractions depending on their log(K_{iw}) values. Among the charged compounds, the seven highest log(K_{iw}) values belong to the PFAS investigated in this study. Thus, our results confirm that remediation efforts based on interfacial processes, such as foam fractionation or reactive micro- and nanobubbles, should be particularly effective for PFAS compounds, in agreement with experimental observations.[106−111]

The boundaries drawn in Figure 6 are sensitive to the water-to-air and water-to-interface ratios of different environmental systems. For example, in an unsaturated soil system with $V_{water}/V_{air} = 3 \times 10^{-1}$, in contrast with the generic cloud with $V_{water}/V_{air} = 3 \times 10^{-7}$ reflected in Figure 6, all three boundaries move to the left by six logarithmic units, placing most compounds predominantly in water. In a system containing ultrafine aqueous aerosol droplets with a 10 nm radius ($V_{water}/A_{interface}$ = 3.3 nm), the boundaries shift downward by three logarithmic units, placing many compounds predominantly at the interface. The finding that many compounds in our study are located within only a few logarithmic units of the horizontal or diagonal boundaries in Figure 6 even in a warm cloud (with low V_{water}/V_{air} and relatively high $V_{water}/A_{interface}$) is consistent with observations that adsorption at water−air interfaces can impact OC behavior in many engineered and natural systems, including during gas stripping,[95] sea spray aerosol emission,[115] and wet deposition.[45]

The configuration used in our MD simulations had $V_{water}/V_{air} \approx 0.5$ (a value typical of unsaturated soils) and $V_{water}/$

https://doi.org/10.1021/acs.est.3c00267
Environ. Sci. Technol. 2023, 57, 6296−6308

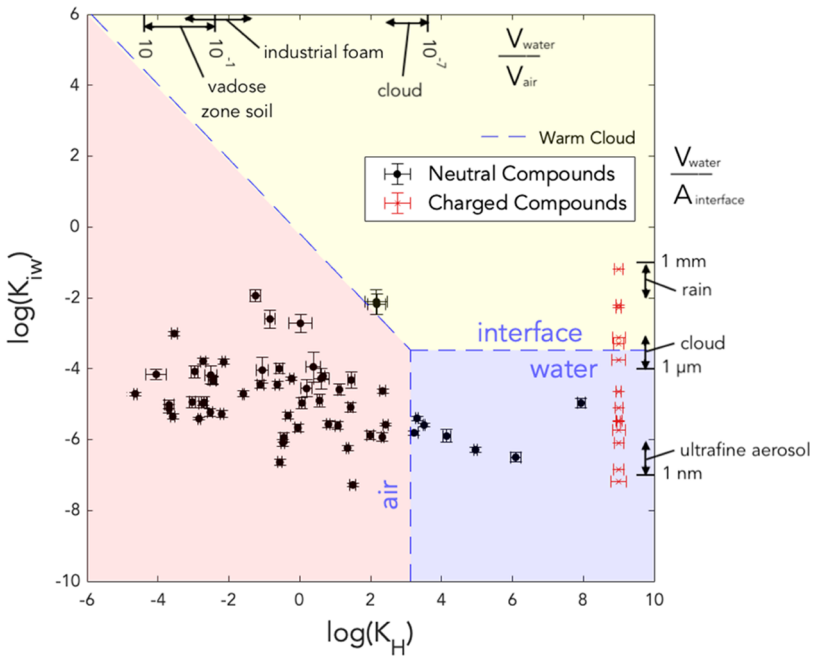

Figure 6. Partitioning space plot[15,105] showing the expected phase in which each compound would primarily be located in a cloud at 298 K (with $V_{water}/V_{air} = 10^{-7}$ and $V_{water}/A_{interface} = 3.3 \times 10^{-6}$ m). Values noted on the left and lower axes indicate the $\log(K_{iw})$ values and bias-corrected $\log(K_H)$ values of each compound as predicted using our MD simulations. Values noted on the right and upper axes indicate the locations in $\log(K_H)-\log(K_{iw})$ space where the three dashed boundaries would intersect in systems with different $V_{water}/A_{interface}$ and V_{water}/V_{air} ratios. Specifically, the $V_{water}/A_{interface}$ ranges indicated along the right axis correspond to different water droplet diameters, with approximate ranges shown for ultrafine aerosols ($\sim 10^{-9}$ to 10^{-8} m), fog droplets ($\sim 10^{-6}$ to 10^{-5} m), and rain droplets ($\sim 10^{-4}$ to 10^{-3} m). The V_{water}/V_{air} ranges along the upper axis correspond to different water saturation levels, with approximate ranges shown for the soil vadose zone (~10 to 90%), industrial foams (~1 to 40%),[112−114] and clouds (<1%).[105]

$A_{interface} \approx 3$ nm (a value typical of ultrafine aerosol particles[116,117] and adsorbed water films on mineral surfaces).[118,119] The corresponding partitioning space plot, presented in Figure SI5, is consistent with our observations that, in unbiased MD simulations of our studied system, most OCs predominantly sample the interfacial region (Figures 1 and SI3).

Implications for Contaminant Fate and Transport. The nearly ubiquitous existence of a FE minimum at the water−air interface indicates that most OCs exhibit higher concentrations at the interface than in either fluid, with potential implications for OC fate, transport, and remediation[5,45,115,120] and for the environmental transformations of natural organic compounds.[90,91] This concentrating effect of the interface is most pronounced for compounds with well-established surfactant properties, such as PFAS,[98,104,115] but remains significant for most other OCs examined here, in agreement with previous studies.[38,45,91,95]

The affinity of most OCs for the interface implies that water−air interfaces in most natural systems carry a significant loading of adsorbed organic molecules. This observation suggests a need to examine how OC adsorption is modulated by pre-existing adsorbed organic substances. Previous studies indicate that cooperative or competitive adsorption at the interface can give rise to relatively complex adsorption trends.[121,122] For instance, PFAS present in mixtures or with other surfactants exhibit sorption isotherms that differ from their monocomponent behavior,[119] with significant impacts on their fate and transport.[123]

Our results also have implications for the adsorption of OCs from air onto solid particles. In this context, relative humidity (RH) has been identified as a significant factor due to the formation of adsorbed water films that compete with OCs for the particle surface.[124−127] Measurements have shown that the adsorption of certain OCs to solid surfaces, such as 2-propanol to activated black carbon[124] and di-n-butyl phthalate (DnBP) to indoor dust,[127] decreases with RH. The relationship does not hold for all OCs, however, as shown by the minimal impact of RH on the adsorption of 1,2,4-trimethylbenzene (1,2,4-TMB) to carbon[124] and di(2-ethylhexyl)phthalate (DEHP) to dust.[127] A potential explanation for the lack of a consistent trend is that adsorbed water may both compete with OCs for adsorption on the dry surface but also create a water−air interface on which OCs can adsorb.

Regarding water treatment, our findings have implications, for example, for the use of micro- and nanobubbles in water purification. These bubbles exhibit an enhancement of reactive oxygen species at the water−air interface that can oxidize OCs.[5,128] Our results suggest that the accumulation of OCs at the interface may enhance the efficiency of associated remediation technologies, as already noted for PFAS.[106,110,111]

Future Research Opportunities. The use of MD simulations to determine partitioning coefficients will likely complement, rather than supplant, existing predictive tools due to the significant time, computational resources, and expertise in molecular modeling required to implement the approach. However, MD simulations provide the notable advantages of providing detailed molecular-scale views of OCs and their coordination in systems in interest, and future establishment of standard simulation routines could greatly reduce the time required. Although the list of compounds examined here remains limited, extension to additional compounds or to

https://doi.org/10.1021/acs.est.3c00267
Environ. Sci. Technol. 2023, 57, 6296−6308

different conditions (e.g., temperature[6] or salinity)[129] should be straightforward. To facilitate such studies, we provide a library of MD simulation input files for the compounds examined here [https://github.com/amelielemay/MD-Contaminants]. We encourage efforts to expand this database; to refine it in the case of compounds identified as outliers, for example, using DFT simulations;[16,130] to use it to evaluate the affinity of OCs for other phases and interfaces;[26,57,131] to evaluate its performance against quantum mechanical approaches;[62] to evaluate the importance of solvent effects in molecular docking simulations;[27,28,132,133] and to apply machine learning approaches to identify clusters and trends within our compound library.[134,135]

■ ASSOCIATED CONTENT

Supporting Information

The Supporting Information is available free of charge at https://pubs.acs.org/doi/10.1021/acs.est.3c00267.

All FE profiles, SPC vs SPC/E model comparison, unbiased vs US simulation comparison, comparison of simulations with and without a charge-balancing ion, all Henry's Law and interfacial adsorption coefficients (K_H, K_{iw}, K_{ia}), and quantitative characteristics of FE profiles (PDF)

■ AUTHOR INFORMATION

Corresponding Author

Amélie C. Lemay − *Department of Civil and Environmental Engineering, Princeton University, Princeton, New Jersey 08544, United States;* orcid.org/0000-0002-4734-8667; Email: alemay@princeton.edu

Authors

Ethan J. Sontarp − *Department of Geosciences, Princeton University, Princeton, New Jersey 08544, United States*

Daniela Martinez − *Department of Civil and Environmental Engineering, Princeton University, Princeton, New Jersey 08544, United States*

Philip Maruri − *Department of Civil and Environmental Engineering, Princeton University, Princeton, New Jersey 08544, United States*

Raneem Mohammed − *Department of Civil and Environmental Engineering, Princeton University, Princeton, New Jersey 08544, United States*

Ryan Neapole − *Department of Civil and Environmental Engineering, Princeton University, Princeton, New Jersey 08544, United States*

Morgan Wiese − *Department of Civil and Environmental Engineering, Princeton University, Princeton, New Jersey 08544, United States*

Jennifer A. R. Willemsen − *Department of Civil and Environmental Engineering, Princeton University, Princeton, New Jersey 08544, United States;* orcid.org/0000-0002-4018-6466

Ian C. Bourg − *Department of Civil and Environmental Engineering, Princeton University, Princeton, New Jersey 08544, United States; High Meadows Environmental Institute, Princeton University, Princeton, New Jersey 08544, United States;* orcid.org/0000-0002-5265-7229

Complete contact information is available at: https://pubs.acs.org/10.1021/acs.est.3c00267

Author Contributions

‖A.C.L. and E.J.S. contributed equally. All authors developed the database of MD simulation input files. A.C.L. and E.J.S. carried out the umbrella sampling simulations and analyzed the results. A.C.L., E.J.S., and I.C.B. wrote the initial manuscript. All authors provided input on the manuscript.

Notes

The authors declare no competing financial interest.

■ ACKNOWLEDGMENTS

This research was supported by the US National Science Foundation under Grant No. CBET 1931611. A.C.L., E.J.S., D.M., P.M., R.M., R.N., and M.W. acknowledge support from the Summer Internship Program of the High Meadows Environmental Institute (HMEI) at Princeton University. A.C.L. and E.J.S. were additionally supported by the Grand Challenges program of the HMEI at Princeton University. Molecular dynamics simulations were performed using resources of the National Energy Research Scientific Computing Center (NERSC), which is supported by the US Department of Energy, Office of Science, under Award DE-AC02-05CH11231, and of the Princeton Institute for Computational Science and Engineering (PICSciE).

■ REFERENCES

(1) Weber, W. J., Jr.; McGinley, P. M.; Katz, L. E. Sorption phenomena in subsurface systems: Concepts, models and effects on contaminant fate and transport. *Water Res.* **1991**, *25*, 499−528.

(2) Schwarzenbach, R. P.; Escher, B. I.; Fenner, K.; Hofstetter, T. B.; Johnson, C. A.; von Gunten, U.; Wehrli, B. The challenge of micropollutants in aquatic systems. *Science* **2006**, *313*, 1072−1077.

(3) Wang, C.; Yuan, T.; Wood, S. A.; Goss, K.-U.; Li, J.; Ying, Q.; Wania, F. Uncertain Henry's law constants compromise equilibrium partitioning calculations of atmospheric oxidation products. *Atmos. Chem. Phys.* **2017**, *17*, 7529−7540.

(4) Li, J.; Sun, X.; Xu, J.; Tan, H.; Zeng, E. Y.; Chen, D. Transplacental transfer of environmental chemicals: Roles of molecular descriptors and placental transporters. *Environ. Sci. Technol.* **2021**, *55*, 519−528.

(5) Lin, J.; Dai, Q.; Zhao, H.; Cao, H.; Wang, T.; Wang, G.; Chen, C. Photoinduced release of volatile organic compounds from fatty alcohols at the air-water interface: The role of singlet oxygen photosensitized by a carbonyl group. *Environ. Sci. Technol.* **2021**, *55*, 8683−8690.

(6) Schwartz-Narbonne, H.; Abbatt, J. P. D.; DeCarlo, P. F.; Farmer, D. K.; Mattila, J. M.; Wang, C.; Donaldson, D. J.; Siegel, J. A. Modeling the removal of water-soluble trace gases from indoor air via air conditioner condensate. *Environ. Sci. Technol.* **2021**, *55*, 10987−10993.

(7) Zhao, F.; Riipinen, I.; MacLeod, M. Steady-state mass balance model for predicting particle-gas concentration ratios of PBDEs. *Environ. Sci. Technol.* **2021**, *55*, 9425−9433.

(8) Wu, S.; Hayati, S. K.; Kim, E.; de la Mata, A. P.; Harynuk, J. J.; Wang, C.; Zhao, R. Henry's law constants and indoor partitioning of microbial volatile organic compounds. *Environ. Sci. Technol.* **2022**, *56*, 7143−7152.

(9) Staikova, M.; Wania, F.; Donaldson, D. J. Molecular polarizability as a single-parameter predictor of vapour pressures and octanol-air partitioning of non-polar compounds: a priori approach and results. *Atmos. Environ.* **2004**, *38*, 213−225.

(10) Wang, Z.; Walker, G. W.; Muir, D. C. G.; Nagatani-Yoshida, K. Toward a global understanding of chemical pollution: a first comprehensive analysis of national and regional chemical inventories. *Environ. Sci. Technol.* **2020**, *54*, 2575−2584.

(11) Persson, L.; Carney Almroth, B. M.; Collins, C. D.; Cornell, S.; de Wit, C. A.; Diamond, M. L.; Fantke, P.; Hassellöv, M.; MacLeod,

M.; Ryberg, M. W.; Jørgensen, P. S.; Villarrubia-Gómez, P.; Wang, Z.; Hauschild, M. Z. Outside the safe operating space of the planetary boundary for novel entities. *Environ. Sci. Technol.* **2022**, *56*, 1510−1521.
(12) United States Environmental Protection Agency. Statistics for the New Chemicals Review Program under TSCA. https://www.epa.gov/reviewing-new-chemicals-under-toxic-substances-control-act-tsca/statistics-new-chemicals-review#pmn (accessed May 11, 2022).
(13) Goss, K.-U.; Schwarzenbach, R. P. Linear free energy relationships used to evaluate equilibrium partitioning of organic compounds. *Environ. Sci. Technol.* **2001**, *35*, 1−9.
(14) Endo, S.; Goss, K.-U. Applications of polyparameter linear free energy relationships in environmental chemistry. *Environ. Sci. Technol.* **2014**, *48*, 12477−12491.
(15) Wania, F.; Lei, Y. D.; Wang, C.; Abbatt, J. P. D.; Goss, K.-U. Using the chemical equilibrium partitioning space to explore factors influencing the phase distribution of compounds involved in secondary organic aerosol formation. *Atmos. Chem. Phys.* **2015**, *15*, 3395−3412.
(16) Li, X.; Chevez, T.; De Silva, A. O.; Muir, D. C. G.; Kleywegt, S.; Simpson, A.; Simpson, M. J.; Jobst, K. J. Which of the (mixed) halogenated n-alkanes are likely to be persistent organic pollutants? *Environ. Sci. Technol.* **2021**, *55*, 15912−15920.
(17) Rodgers, T. F. M.; Okeme, J. O.; Parnis, J. M.; Girdhari, K.; Bidleman, T. F.; Wan, Y.; Jantunen, L. M.; Diamond, M. L. Novel Bayesian method to derive final adjusted values of physicochemical properties: Application to 74 compounds. *Environ. Sci. Technol.* **2021**, *55*, 12302−12316.
(18) Endo, S. Applicability domain of polyparameter linear free energy relationship models evaluated by leverage and prediction interval calculation. *Environ. Sci. Technol.* **2022**, *56*, 5572−5579.
(19) Klamt, A.; Eckert, F. COSMO-RS: A novel and efficient method for the a priori prediction of thermophysical data of liquids. *Fluid Phase Equilib.* **2000**, *172*, 43−72.
(20) Klamt, A.; Eckert, F.; Arlt, W. COSMO-RS: An alternative to simulation for calculating thermodynamic properties of liquid mixtures. *Annu. Rev. Chem. Biomol. Eng.* **2010**, *1*, 101−122.
(21) Roth, C. M.; Goss, K.-U.; Schwarzenbach, R. P. Adsorption of a diverse set of organic vapors on the bulk water surface. *J. Colloid Interface Sci.* **2002**, *252*, 21−30.
(22) Hyttinen, N.; Wolf, M.; Rissanen, M. P.; Ehn, M.; Peräkylä, O.; Kurtén, T.; Prisle, N. L. Gas-to-particle partitioning of cyclohexene- and α-pinene-derived highly oxygenated dimers evaluated using COSMO*therm*. *J. Phys. Chem. A* **2021**, *125*, 3726−3728.
(23) Overdahl, K. E.; Sutton, R.; Sun, J.; DeStefano, N. J.; Getzinger, G. J.; Ferguson, P. L. Assessment of emerging polar organic pollutants linked to contaminant pathways within an urban estuary using non-targeted analysis. *Environ. Sci.: Processes Impacts* **2021**, *23*, 429−445.
(24) Sliwoski, G.; Kothiwale, S.; Meiler, J.; Lowe, E. W., Jr. Computational methods in drug discovery. *Pharmacol. Rev.* **2014**, *66*, 334−395.
(25) De Vivo, M.; Masetti, M.; Bottegoni, G.; Cavalli, A. Role of molecular dynamics and related methods in drug discovery. *J. Med. Chem.* **2016**, *59*, 4035−4061.
(26) Holmboe, M.; Larsson, P.; Anwar, J.; Bergström, C. A. S. Partitioning into colloidal structures of fasted state intestinal fluid studied by molecular dynamics simulations. *Langmuir* **2016**, *32*, 12732−12740.
(27) Peng, W.; Ding, F.; Peng, Y.-K. *In vitro* evaluation of the conjugations of neonicotinoids with transport protein: photochemistry, ligand docking and molecular dynamics studies. *RSC Adv.* **2016**, *6*, 1826−1843.
(28) Yan, J.; Yan, X.; Hu, S.; Zhu, H.; Yan, B. Comprehensive interrogation on acetylcholinesterase inhibition by ionic liquids using machine learning and molecular modeling. *Environ. Sci. Technol.* **2021**, *55*, 14720−14731.
(29) Kubicki, J. D. Molecular simulations of benzene and PAH interactions with soot. *Environ. Sci. Technol.* **2006**, *40*, 2298−2303.
(30) Tribe, L.; Kwon, K. D.; Trout, C. C.; Kubicki, J. D. Molecular orbital theory study on surface complex structures of glyphosate on goethite: calculation of vibrational frequencies. *Environ. Sci. Technol.* **2006**, *40*, 3836−3841.
(31) Lock, P. A.; Skipper, N. T. Computer simulation of the structure and dynamics of phenol in sodium montmorillonite hydrates. *Eur. J. Soil Sci.* **2007**, *58*, 958−966.
(32) Lim, D.-H.; Lastoskie, C. M.; Soon, A.; Becker, U. Density functional theory studies of chloroethene adsorption on zerovalent iron. *Environ. Sci. Technol.* **2009**, *43*, 1192−1198.
(33) Zhou, Q.; Zhu, R.; Parker, S. C.; Zhu, J.; He, H.; Molinari, M. Modelling the effects of surfactant loading level on the sorption of organic contaminants on organoclays. *RSC Adv.* **2015**, *5*, 47022−47030.
(34) Okaikue-Woodi, F. E. K.; Kelch, S. E.; Schmidt, M. P.; Martinez, C. E.; Youngman, R. E.; Aristilde, L. Structures and mechanisms in clay nanopore trapping of structurally-different fluoroquinolone antimicrobials. *J. Colloid Interface Sci.* **2018**, *513*, 367−378.
(35) Loganathan, N.; Wilson, A. K. Adsorption, structure, and dynamics of short- and long-chain PFAS molecules in kaolinite: molecular-level insights. *Environ. Sci. Technol.* **2022**, *56*, 8043−8052.
(36) Ahmed, A.; Sandler, S. I. Hydration free energies of multifunctional nitroaromatic compounds. *J. Chem. Theory Comput.* **2013**, *9*, 2774−2785.
(37) Bhatnagar, N.; Kamath, G.; Potoff, J. J. Prediction of 1-octanol-water and air-water partition coefficients for nitro-aromatic compounds from molecular dynamics simulations. *Phys. Chem. Chem. Phys.* **2013**, *15*, 6467−6474.
(38) Habartová, A.; Valsaraj, K. T.; Roeselová, M. Molecular dynamics simulations of small halogenated organics at the air-water interface: implications in water treatment and atmospheric chemistry. *J. Phys. Chem. A* **2013**, *117*, 9205−9215.
(39) Shapley, T. V.; Molinari, M.; Zhu, R.; Parker, S. C. Atomistic modeling of the sorption free energy of dioxins at clay-water interfaces. *J. Phys. Chem. C* **2013**, *117*, 24975−24984.
(40) Willemsen, J. A. R.; Myneni, S. C. B.; Bourg, I. C. Molecular dynamics simulations of the adsorption of phthalate esters on smectite clay surfaces. *J. Phys. Chem. C* **2019**, *123*, 13624−13636.
(41) Willemsen, J. A. R.; Bourg, I. C. Molecular dynamics simulation of the adsorption of per- and polyfluoroalkyl substances (PFASs) on smectite clay. *J. Colloid Interface Sci.* **2021**, *585*, 337−346.
(42) Luft, C. M.; Schutt, T. C.; Shukla, M. K. Properties and mechanisms for PFAS adsorption to aqueous clay and humic soil components. *Environ. Sci. Technol.* **2022**, *56*, 10053−10061.
(43) Goss, K.-U.; Schwarzenbach, R. P. Gas/solid and gas/liquid partitioning of organic compounds: Critical evaluation of the interpretation of equilibrium constants. *Environ. Sci. Technol.* **1998**, *32*, 2025−2032.
(44) Brusseau, M. L.; Guo, B.; Huang, D.; Yan, N.; Lyu, Y. Ideal versus nonideal transport of PFAS in unsaturated porous media. *Water Res.* **2021**, *202*, No. 117405.
(45) Casas, G.; Martinez-Varela, A.; Vila-Costa, M.; Jiménez, B.; Dachs, J. Rain amplification of persistent organic pollutants. *Environ. Sci. Technol.* **2021**, *55*, 12961−12972.
(46) Calafat, A. M.; Wong, L.-Y.; Kuklenyik, Z.; Reidy, J. A.; Needham, L. L. Polyfluoroalkyl Chemicals in the U.S. Population: Data from the National Health and Nutrition Examination Survey (NHANES) 2003-2004 and Comparisons with NHANES 1999-2000. *Environ. Health Perspect.* **2007**, *115*, 1596−1602.
(47) Sunderland, E. M.; Hu, X. C.; Dassuncao, C.; Tokranov, A. K.; Wagner, C. C.; Allen, J. G. A review of the pathways of human exposure to poly- and perfluroroalkyl substances (PFASs) and present understanding of health effects. *J. Exposure Sci. Environ. Epidemiol.* **2019**, *29*, 131−147.
(48) Ortiz de García, S. A.; Pinto, G. P.; Garcìa-Encina, P. A.; Irusta-Mata, R. Ecotoxicity and environmental risk assessment of pharmaceuticals and personal care products in aquatic environments and wastewater treatment plants. *Ecotoxicology* **2014**, *23*, 1517−1533.

https://doi.org/10.1021/acs.est.3c00267
Environ. Sci. Technol. 2023, 57, 6296−6308

(49) Wojcieszyńska, D.; Guzik, U. Naproxen in the environment: its occurrence, toxicity to nontarget organisms and biodegradation. *Appl. Microbiol. Biotechnol.* **2020**, *104*, 1849−1857.
(50) Wormuth, M.; Scheringer, M.; Vollenweider, M.; Hungerbühler, K. What are the sources of exposure to eight frequently used phthalic acid esters in Europeans? *Risk Anal.* **2006**, *26*, 803−824.
(51) Dutta, S.; Haggerty, D. K.; Rappolee, D. A.; Ruden, D. M. Phthalate exposure and long-term epigenomic consequences: a review. *Front. Genet.* **2020**, *11*, 405.
(52) Boyle, M. D.; Kavi, L. K.; Louis, L. M.; Pool, W.; Sapkota, A.; Zhu, L.; Pollack, A. Z.; Thomas, S.; Rule, A. M.; Quirós-Alcalá, L. Occupational exposures to phthalates among Black and Latina U.S. hairdressers serving an ethnically diverse clientele: A pilot study. *Environ. Sci. Technol.* **2021**, *55*, 8128−8138.
(53) Geier, M. C.; Chebowski, A. C.; Truong, L.; Massey Simonich, S. L.; Anderson, K. A.; Tanguay, R. L. Comparative developmental toxicity of a comprehensive suite of polycyclic aromatic hydrocarbons. *Arch. Toxicol.* **2018**, *92*, 571−586.
(54) Patel, A. B.; Shaikh, S.; Jain, K. R.; Desai, C.; Madamwar, D. Polycyclic aromatic hydrocarbons: sources, toxicity, and remediation approaches. *Front. Microbiol.* **2020**, *11*, No. 562813.
(55) Lohmann, R.; Markham, E.; Klanova, J.; Kukucka, P.; Pribylova, P.; Gong, X.; Pockalny, R.; Yanishevsky, T.; Wagner, C. C.; Sunderland, E. M. Trends of diverse POPs in air and water across the Western Atlantic Ocean: Strong gradients in the ocean but not in the air. *Environ. Sci. Technol.* **2021**, *55*, 9498−9507.
(56) Bannavti, M. K.; Jahnke, J. C.; Marek, R. F.; Just, C. L.; Hornbuckle, K. C. Room-to-room variability of airborne polychlorinated biphenyls in schools and the application of air sampling for targeted source evaluation. *Environ. Sci. Technol.* **2021**, *55*, 9460−9468.
(57) Muñoz, C. C.; Hendriks, A. J.; Ragas, A. M. J.; Vermeiren, P. Internal and maternal distribution of persistent organic pollutants in sea turtle tissues: A meta-analysis. *Environ. Sci. Technol.* **2021**, *55*, 10012−10024.
(58) Schuster, J. K.; Harner, T.; Eng, A.; Rauert, C.; Su, K.; Hornbuckle, K. C.; Johnson, C. W. Tracking POPs in global air from the first 10 years of the GAPS network (2005 to 2014). *Environ. Sci. Technol.* **2021**, *55*, 9479−9488.
(59) Jackson, J.; Sutton, R. Sources of endocrine-disrupting chemicals in urban wastewater, Oakland, CA. *Sci. Total Environ.* **2008**, *405*, 153−160.
(60) Chen, D.; Kannan, K.; Tan, H.; Zheng, Z.; Feng, Y.-L.; Wu, Y.; Widelka, M. Bisphenol analogues other than BPA: Environmental occurrence, human exposure, and toxicity—A review. *Environ. Sci. Technol.* **2016**, *50*, 5438−5453.
(61) Geer, L. A.; Pycke, B. F. G.; Waxenbaum, J.; Sherer, D. M.; Abulafia, O.; Halden, R. U. Association of birth outcomes with fetal exposure to parabens, triclosan and triclocarban in an immigrant population in Brooklyn, New York. *J. Hazard. Mater.* **2017**, *323*, 177−183.
(62) Salthammer, T.; Grimme, S.; Stahn, M.; Hohm, U.; Palm, W.-U. Quantum chemical calculation and evaluation of partition coefficients for classical and emerging environmentally relevant organic compounds. *Environ. Sci. Technol.* **2022**, *56*, 379−391.
(63) Shimabuku, I.; Chen, D.; Wu, Y.; Miller, E.; Sun, J.; Sutton, R. Occurrence and risk assessment of organophosphate esters and bisphenols in San Francisco Bay, California, USA. *Sci. Total Environ.* **2022**, *813*, No. 152287.
(64) McNeill, V. F. Aqueous organic chemistry in the atmosphere: Sources and chemical processing of organic aerosols. *Environ. Sci. Technol.* **2015**, *49*, 1237−1244.
(65) Wang, C.; Collins, D. B.; Arata, C.; Goldstein, A. H.; Mattila, J. M.; Farmer, D. K.; Ampollini, L.; DeCarlo, P. F.; Novoselac, A.; Vance, M. E.; Nazaroff, W. W.; Abbatt, J. P. D. Surface reservoirs dominate dynamic gas-surface partitioning of many indoor air constituents. *Sci. Adv.* **2020**, *6*, No. eaay8973.
(66) Jorgensen, W. L.; Maxwell, D. S.; Tirado-Rives, J. Development and testing of the OPLS all-atom force field on conformational energetics and properties of organic liquids. *J. Am. Chem. Soc.* **1996**, *118*, 11225−11236.
(67) Jorgensen, W. L.; Tirado-Rives, J. Potential energy functions for atomic-level simulations of water and organic and biomolecular systems. *Proc. Natl. Acad. Sci. U.S.A.* **2005**, *102*, 6665−6670.
(68) Jewett, A. I.; Stelter, D.; Lambert, J.; Saladi, S. M.; Roscioni, O. M.; Ricci, M.; Autin, L.; Maritan, M.; Bashusqeh, S. M.; Keyes, T.; Dame, R. T.; Shea, J.-E.; Jensen, G. J.; Goodsell, D. S. Moltemplate: A tool for coarse-grained modeling of complex biological matter and soft condensed matter physics. *J. Mol. Biol.* **2021**, *433*, No. 166841.
(69) Plimpton, S. Fast parallel algorithm for short-range molecular dynamics. *J. Comput. Phys.* **1995**, *117*, 1−19.
(70) Eastwood, J. W.; Hockney, R. W.; Lawrence, D. N. P3M3DP − The three-dimensional periodic particle-particle/particle-mesh program. *Comput. Phys. Commun.* **1980**, *19*, 215−261.
(71) Ryckaert, J.-P.; Ciccotti, G.; Berendsen, H. J. C. Numerical integration of the cartesian equations of motion of a system with constraints: Molecular dynamics of n-alkanes. *J. Comput. Phys.* **1977**, *23*, 327−341.
(72) Allen, M. P.; Tildesley, D. J. *Computer Simulation of Liquids*; Oxford University Press, 1987.
(73) Smith, D. E.; Dang, L. X. Computer simulations of NaCl association in polarizable water. *J. Chem. Phys.* **1994**, *100*, 3757−3766.
(74) Berendsen, H. J. C.; Postma, J. P. M.; van Gunsteren, W. F.; Hermans, J. Interaction Models for Water in Relation to Protein Hydration. In *Intermolecular Forces*; Pullman, B., Ed.; Reidel, 1981; pp 331−342.
(75) Ponder, J. W.; Case, D. A. Force fields for protein simulations. *Adv. Protein Chem.* **2003**, *66*, 27−85.
(76) Shivakumar, D.; Williams, J.; Wu, Y.; Damm, W.; Shelley, J.; Sherman, W. Prediction of absolute solvation free energies using molecular dynamics free energy perturbation and the OPLS force field. *J. Chem. Theory Comput.* **2010**, *6*, 1509−1519.
(77) Hub, J. S.; Caleman, C.; van der Spoel, D. Organic molecules on the surface of water droplets − an energetic perspective. *Phys. Chem. Chem. Phys.* **2012**, *14*, 9537−9545.
(78) Stroet, M.; Caron, B.; Visscher, K. M.; Geerke, D. P.; Malde, A. K.; Mark, A. E. Automated topology builder version 3.0: prediction of solvation free enthalpies in water and hexane. *J. Chem. Theory Comput.* **2018**, *14*, 5834−5845.
(79) Berendsen, H. J. C.; Grigera, J. R.; Straatsma, T. P. The missing term in effective pair potentials. *J. Phys. Chem. A* **1987**, *91*, 6269−6271.
(80) Salomon-Ferrer, R.; Case, D. A.; Walker, R. C. An overview of the Amber biomolecular simulation package. *WIREs Comput. Mol. Sci.* **2013**, *3*, 198−210.
(81) Vanommeslaeghe, K.; Hatcher, E.; Acharya, C.; Kundu, S.; Zhong, S.; Shim, J.; Darian, E.; Guvench, O.; Lopes, P.; Vorobyov, I.; Mackerell, A. D., Jr. CHARMM general force field: A force field for drug-like molecules compatible with the CHARMM all-atom additive biological force fields. *J. Comput. Chem.* **2010**, *31*, 671−690.
(82) Oostenbrink, C.; Villa, A.; Mark, A. E.; Van Gunsteren, W. F. A biomolecular force field based on the free enthalpy of hydration and solvation: The GROMOS force-field parameter sets 53A5 and 53A6. *J. Comput. Chem.* **2004**, *25*, 1656−1676.
(83) Abascal, J. L. F.; Vega, C. A general purpose model for the condensed phases of water: TIP4P/2005. *J. Chem. Phys.* **2005**, *123*, No. 234505.
(84) Torrie, G. M.; Valleau, J. P. Nonphysical sampling distributions in Monte Carlo free-energy estimation: Umbrella sampling. *J. Comput. Phys.* **1977**, *23*, 187−199.
(85) Kumar, S.; Bouzida, D.; Swendsen, R. H.; Kollman, P. A.; Rosenberg, J. M. The weighted histogram analysis method for free-energy calculations on biomolecules. I. The method. *J. Comput. Chem.* **1992**, *13*, 1011−1021.

https://doi.org/10.1021/acs.est.3c00267
Environ. Sci. Technol. 2023, 57, 6296−6308

(86) Loche, P.; Bonthuis, D. J.; Netz, R. R. Molecular dynamics simulations of the evaporation of hydrated ions from aqueous solution. *Commun. Chem.* **2022**, *5*, 55.
(87) Kikkawa, N.; Wang, L.; Morita, A. Microscopic barrier mechanism of ion transport through liquid-liquid interface. *J. Am. Chem. Soc.* **2015**, *137*, 8022−8025.
(88) Karnes, J. J.; Benjamin, I. Geometric and energetic considerations of surface fluctuations during ion transfer across the water-immiscible organic liquid interface. *J. Chem. Phys.* **2016**, *145*, No. 014701.
(89) Wang, H.; Zhao, X.; Eisenthal, K. B. Effects of monolayer density and bulk ionic strength on acid-base equilibria at the air/water interface. *J. Phys. Chem. B* **2000**, *104*, 8855−8861.
(90) Donaldson, D. J.; Vaida, V. The influence of organic films at the air-aqueous boundary on atmospheric processes. *Chem. Rev.* **2006**, *106*, 1445−1461.
(91) Kolb, C. E.; Cox, R. A.; Abbatt, J. P. D.; Ammann, M.; Davis, E. J.; Donaldson, D. J.; Garrett, B. C.; George, C.; Griffiths, P. T.; Hanson, D. R.; Kulmala, M.; McFiggans, G.; Pöschl, U.; Riipinen, I.; Rossi, M. J.; Rudich, Y.; Wagner, P. E.; Winkler, P. M.; Worsnop, D. R.; O'Dowd, C. D. An overview of current issues in the uptake of atmospheric trace gases by aerosols and clouds. *Atmos. Chem. Phys.* **2010**, *10*, 10561−10605.
(92) Willard, A. P.; Chandler, D. Instantaneous liquid interfaces. *J. Phys. Chem. B* **2010**, *114*, 1954−1958.
(93) Shiraiwa, M.; Pfrang, C.; Koop, T.; Pöschl, U. Kinetic multi-layer model of gas-particle interactions in aerosols and clouds (KM-GAP): linking condensation, evaporation and chemical reactions of organics, oxidants and water. *Atmos. Chem. Phys.* **2012**, *12*, 2777−2794.
(94) Sander, R. Compilation of Henry's law constants (version 4.0) for water as solvent. *Atmos. Chem. Phys.* **2015**, *15*, 4399−4981.
(95) Shunthirasingham, C.; Lei, Y. D.; Wania, F. Evidence of bias in air-water Henry's law constants for semivolatile organic compounds measured by inert gas stripping. *Environ. Sci. Technol.* **2007**, *41*, 3807−3814.
(96) Shunthirasingham, C.; Cao, X.; Lei, Y. D.; Wania, F. Large bubbles reduce the surface sorption artifact of the inert gas stripping method. *J. Chem. Eng. Data* **2013**, *58*, 792−797.
(97) Hoff, J. T.; Mackay, D.; Gillham, R.; Shiu, W. Y. Partitioning of organic chemicals at the air-water interface in environmental systems. *Environ. Sci. Technol.* **1993**, *27*, 2174−2180.
(98) Brusseau, M. L. The influence of molecular structure on the adsorption of PFAS to fluid-fluid interfaces: Using QSPR to predict interfacial adsorption coefficients. *Water Res.* **2019**, *152*, 148−158.
(99) Kelly, C. P.; Cramer, C. J.; Truhlar, D. G. Predicting adsorption coefficients at air-water interfaces using universal solvation and surface area models. *J. Phys. Chem. B* **2004**, *108*, 12882−12897.
(100) Hansen, N.; van Gunsteren, W. F. Practical aspects of free-energy calculations: a review. *J. Chem. Theory Comput.* **2014**, *10*, 2632−2647.
(101) Schaefer, C. E.; Culina, V.; Nguyen, D.; Field, J. Uptake of poly- and perfluoroalkyl substances at the air-water interface. *Environ. Sci. Technol.* **2019**, *53*, 12442−12448.
(102) Arshadi, M.; Costanza, J.; Abriola, L. M.; Pennell, K. D. Comment on "Uptake of poly- and perfluoroalkyl substances at the air-water interface". *Environ. Sci. Technol.* **2020**, *54*, 7019−7020.
(103) Schaefer, C. E.; Nguyen, D.; Field, J. Response to the comment on "Uptake of poly- and perfluoroalkyl substances at the air-water interface". *Environ. Sci. Technol.* **2020**, *54*, 7021−7022.
(104) Stults, J. F.; Choi, Y. J.; Schaefer, C. E.; Illangasekare, T. H.; Higgins, C. P. Estimation of transport parameters of perfluoroalkyl acids (PFAAs) in unsaturated porous media: critical experimental and modeling improvements. *Environ. Sci. Technol.* **2022**, *56*, 7963−7975.
(105) Lei, Y. D.; Wania, F. Is rain or snow a more efficient scavenger of organic chemicals? *Atmos. Environ.* **2004**, *38*, 3557−3571.
(106) Takeuchi, N.; Kitagawa, Y.; Kosugi, A.; Tachibana, K.; Obo, H.; Yasuoka, K. Plasma-liquid interfacial reaction in decomposition of perfluoro surfactants. *J. Phys. D: Appl. Phys.* **2014**, *47*, No. 045203.
(107) Ebersbach, I.; Ludwig, S. M.; Constapel, M.; Kling, H.-W. An alternative treatment method for fluorosurfactant-containing wastewater by aerosol-mediated separation. *Water Res.* **2016**, *101*, 333−340.
(108) Meng, P.; Deng, S.; Maimaiti, A.; Wang, B.; Huang, J.; Wang, Y.; Cousins, I. T.; Yu, G. Efficient removal of perfluorooctane sulfonate from aqueous film-forming foam solution by aeration-foam collection. *Chemosphere* **2018**, *203*, 263−270.
(109) Robey, N. M.; da Silva, B. F.; Annable, M. D.; Townsend, T. G.; Bowden, J. A. Concentrating per- and polyfluoroalkyl substances (PFAS) in municipal solid waste landfill leachate using foam separation. *Environ. Sci. Technol.* **2020**, *54*, 12550−12559.
(110) Jiang, X.; Wang, W.; Yu, G.; Deng, S. Contribution of nanobubbles for PFAS adsorption on graphene and OH- and NH_2-functionalized graphene: comparing simulations with experimental results. *Environ. Sci. Technol.* **2021**, *55*, 13254−13263.
(111) Zhang, H.; Li, P.; Zhang, A.; Sun, Z.; Liu, J.; Héroux, P.; Liu, Y. Enhancing interface reactions by introducing microbubbles into a plasma treatment process for efficient decomposition of PFOA. *Environ. Sci. Technol.* **2021**, *55*, 16067−16077.
(112) Eftekhari, A. A.; Farajzadeh, R. Effect of Foam on Liquid Phase Mobility in Porous Media. *Sci. Rep.* **2017**, *7*, No. 43870.
(113) Skauge, A.; Solbakken, J.; Ormehaug, P. A.; Aarra, M. G. Foam Generation, Propagation and Stability in Porous Medium. *Transp. Porous Media* **2020**, *131*, 5−21.
(114) Li, K.; Wolf, K.-H. A. A.; Rossen, W. R. A novel technique to estimate water saturation and capillary pressure of foam in model fractures. *Colloids Surf., A* **2022**, *632*, No. 127800.
(115) Sha, B.; Johansson, J. H.; Benskin, J. P.; Cousins, I. T.; Salter, M. E. Influence of water concentrations of perfluoroalkyl acids (PFAAs) on their size-resolved enrichment in nascent sea spray aerosols. *Environ. Sci. Technol.* **2021**, *55*, 9489−9497.
(116) Kontkanen, J.; Lehtipalo, K.; Ahonen, L.; Kangasluoma, J.; Manninen, H. E.; Hakala, J.; Rose, C.; Sellegri, K.; Xiao, S.; Wang, L.; Qi, X.; Nie, W.; Ding, A.; Yu, H.; Lee, S.; Kerminen, V.-M.; Petäjä, T.; Kulmala, M. Measurements of sub-3 nm particles using a particle size magnifier in different environments: from clean mountain top to polluted megacities. *Atmos. Chem. Phys.* **2017**, *17*, 2163−2187.
(117) Deng, C.; Fu, Y.; Dada, L.; Yan, C.; Cai, R.; Yang, D.; Zhou, Y.; Yin, R.; Lu, Y.; Li, X.; Qiao, X.; Fan, X.; Nie, W.; Kontkanen, J.; Kangasluoma, J.; Chu, B.; Ding, A.; Kerminen, V.-M.; Paasonen, P.; Worsnop, D. R.; Bianchi, F.; Liu, Y.; Zheng, J.; Wang, L.; Kulmala, M.; Jiang, J. Seasonal characteristics of new particle formation and growth in urban Beijing. *Environ. Sci. Technol.* **2020**, *54*, 8547−8557.
(118) Rubasinghege, G.; Grassian, V. H. Role(s) of adsorbed water in the surface chemistry of environmental interfaces. *Chem. Commun.* **2013**, *49*, 3071−3094.
(119) Yalcin, S. E.; Legg, B. A.; Yesilbas, M.; Malvankar, N. S.; Boily, J.-F. Direct observation of anisotropic growth of water films on minerals driven by defects and surface tension. *Sci. Adv.* **2020**, *6*, No. eaaz9708.
(120) Sha, B.; Johansson, J. H.; Tunved, P.; Bohlin-Nizzetto, P.; Cousins, I. T.; Salter, M. E. Sea spray aerosol (SSA) as a source of perfluoroalkyl acids (PFAAs) to the atmosphere: field evidence from long-term air monitoring. *Environ. Sci. Technol.* **2022**, *56*, 228−238.
(121) Minofar, B.; Vácha, R.; Wahab, A.; Mahiuddin, S.; Kunz, W.; Jungwirth, P. Propensity for the air/water interface and ion pairing in magnesium acetate vs. magnesium nitrate solutions: Molecular dynamics simulations and surface tension measurements. *J. Phys. Chem. B* **2006**, *110*, 15939−15944.
(122) Silva, J. A. K.; Martin, W. A.; McCray, J. E. Air-water interfacial adsorption coefficients for PFAS when present as a multi-component mixture. *J. Contam. Hydrol.* **2021**, *236*, No. 103731.
(123) Ji, Y.; Yan, N.; Brusseau, M. L.; Guo, B.; Zheng, X.; Dai, M.; Liu, H.; Li, X. Impact of a hydrocarbon surfactant on the retention and transport of perfluorooctanoic acid in saturated and unsaturated porous media. *Environ. Sci. Technol.* **2021**, *55*, 10480−10490.
(124) Laskar, I. I.; Hashisho, Z.; Philips, J. H.; Anderson, J. E.; Nichols, M. Modeling the effect of relative humidity on adsorption

https://doi.org/10.1021/acs.est.3c00267
Environ. Sci. Technol. 2023, 57, 6296−6308

dynamics of volatile organic compound onto activated carbon. *Environ. Sci. Technol.* **2019**, *53*, 2647−2659.
(125) Wu, Y.; Venier, M.; Salamova, A. Spatioseasonal variations and partitioning behavior of organophosphate esters in the Great Lakes atmosphere. *Environ. Sci. Technol.* **2020**, *54*, 5400−5408.
(126) Yaman, B.; Dumanoglu, Y.; Odabasi, M. Measurement and modeling the phase partitioning of organophosphate esters using their temperature-dependent octanol-air partition coefficients and vapor pressures. *Environ. Sci. Technol.* **2020**, *54*, 8133−8143.
(127) Bi, C.; Wang, X.; Li, H.; Li, X.; Xu, Y. Direct transfer of phthalate and alternative plasticizers from indoor source products to dust: Laboratory measurements and predictive modeling. *Environ. Sci. Technol.* **2021**, *55*, 341−351.
(128) Wu, J.; Zhang, K.; Cheng, C.; Wu, X.; Mao, R.; Zheng, Y. Role of bulk nanobubbles in removing organic pollutants in wastewater treatment. *AMB Express* **2021**, *11*, 96.
(129) Costanza, J.; Arshadi, M.; Abriola, L. M.; Pennell, K. D. Accumulation of PFOA and PFOS at the air-water interface. *Environ. Sci. Technol. Lett.* **2019**, *6*, 487−491.
(130) Lewer, J.; Huang, J.; Peloquin, J.; Kostal, J. Structure-energetics-property relationships support computational design of photodegradable pesticides. *Environ. Sci. Technol.* **2021**, *55*, 11713−11722.
(131) Gschwend, P.; MacFarlane, J.; Jensen, D.; Soo, J.; Saparbaiuly, G.; Borrelli, R.; Vago, F.; Oldani, A.; Zaninetta, L.; Verginelli, I.; Baciocchi, R. *In situ* equilibrium polyethylene passive sampling of soil gas VOC concentrations: modeling, parameter determinations, and laboratory testing. *Environ. Sci. Technol.* **2022**, *56*, 7810−7819.
(132) Tan, H.; Chen, Q.; Hong, H.; Benfenati, E.; Gini, G. C.; Zhang, X.; Yu, H.; Shi, W. Structures of endocrine-disrupting chemicals correlate with the activation of 12 classic nuclear receptors. *Environ. Sci. Technol.* **2021**, *55*, 16552−16562.
(133) Scott, S. E.; Fernandez, J. P.; Hadad, C. M.; MacKay, A. A. Molecular docking as a tool to examine organic cation sorption to organic matter. *Environ. Sci. Technol.* **2022**, *56*, 951−961.
(134) Gao, F.; Shen, Y.; Sallach, J. B.; Li, H.; Liu, C.; Li, Y. Direct prediction of bioaccumulation of organic contaminants in plant roots from soils with machine learning models based on molecular structures. *Environ. Sci. Technol.* **2021**, *55*, 16358−16368.
(135) Zhong, S.; Zhang, K.; Bagheri, M.; Burken, J. G.; Gu, A.; Li, B.; Ma, X.; Marrone, B. L.; Ren, Z. J.; Schrier, J.; Shi, W.; Tan, H.; Wang, T.; Wang, X.; Wong, B. M.; Xiao, X.; Yu, X.; Zhu, J.-J.; Zhang, H. Machine learning: new ideas and tools in environmental science and engineering. *Environ. Sci. Technol.* **2021**, *55*, 12741−12754.

https://doi.org/10.1021/acs.est.3c00267
Environ. Sci. Technol. 2023, 57, 6296−6308